Applied Catalysis A: General 419–420 (2012) 102–110

Contents lists available at SciVerse ScienceDirect

Applied Catalysis A: General

journal homepage: www.elsevier.com/locate/apcata

Catalytic fast pyrolysis of furfural over H-ZSM-5 and Zn/H-ZSM-5 catalysts

Wei-Liang Fanchiang, Yu-Chuan Lin*

Department of Chemical Engineering and Materials Science, Yuan Ze University, Chungli, Taoyuan 32003 Taiwan

ARTICLE INFO

Article history:
Received 14 November 2011
Received in revised form 13 January 2012
Accepted 15 January 2012
Available online 25 January 2012

Keywords:
Fast pyrolysis
Furfural
Zeolite
Biofuels
ZSM-5

ABSTRACT

Furfural, a cellulose model compound, was converted into gasoline-range fuels through catalytic fast pyrolysis. H-ZSM-5-based catalysts were employed in a continuous fixed bed system. The reaction temperature, reactant contact time, and catalytic promoter are keys to manipulate the product distribution. The first step in furfural conversion is the decarbonylation of furfural to form furan, followed by furan conversion to intermediates (e.g., cyclohexene and 3,4-dimethylbenzaldehyde) in the ZSM-5 pores. These intermediates can then be transformed into aromatics, coke, light olefins, and carbon oxides. A reaction temperature of 500 °C generated the highest yield of aromatics and the lowest amount of coke. A long contact time (~1.5 s) also provided the highest aromatic selectivity. The promoter, zinc oxide, plays an important role in hydrogen atom transfer. This is attributed to the change of acid site concentration and Lewis acid sites created by anchored Zn ions.

1. Introduction

The conversion of lignocellulosic biomass has the potential to be a renewable and carbon neutral method of producing fuels and chemicals [1–3]. Several groups have recently developed novel technologies, such as reactive flash volatilization [4,5] and catalytic fast pyrolysis [6,7], to overcome the difficulty of lignocellulosic biomass processing. The first step of these approaches is to disintegrate the solid lignocellulosic frameworks into reactive intermediates, which can then be transformed into desired products.

Furfural is a common intermediate in various biorefining processes. Woody biomass pyrolysis yields furfural in the form of dehydrated products from cellulose and hemicellulose [8–10]. Bio-oils derived from biomass liquefaction also contain significant amounts of furfural [2,11]. Thus, furfural is a popular model compound of lignocellulosic derivatives. For example, Elliott and Hart used furfural as a cellulosic model compound in the catalytic hydroprocessing of a bio-oil-like mixture [12]. An effective method of furfural conversion should facilitate lignocellulosic biorefining.

Hydrogenation and aqueous phase processing are currently the two most encountered approaches of converting furfural into fuel-grade chemicals [2]. The major products of furfural hydrogenation are furfuryl alcohol, methylfuran, tetrahydrofurfuryl alcohol, and methyltetrahydrofuran (MTHF) [2], which is a key component in P-Series fuels [13]. Aqueous phase processing allows furfural to couple with acetone to form dimers through aldol-condensation. A series of hydrodeoxygenation steps can then transform these dimers into gasoline-range alkanes (C_7–C_{15}) [14–16].

Pyrolysis in the presence of zeolites is another method for biomass upgrading that involves oxygen removal through a series of dehydration, decarbonylation, and decarboxylation reactions. This process was introduced in Mobil's pioneering research on methanol-to-gasoline (MTG) production [17–19]. Chen et al. [20] showed that ZSM-5-based catalysts can convert glucose solutions into olefins and aromatics. Diebold et al. [21,22] invented an integrated process of fast pyrolysis with catalytic cracking to upgrade pyrolysis vapors. Their research stimulated follow-up studies on reactor design [23–26].

Zeolite design for biomass pyrolysis is another common research topic. A research group at the University of Saskatchewan investigated the performance of various zeolites in bio-oil upgrading [27–29]. Zeolites selection for lignocellulosics pyrolysis has recently been investigated in numerous institutes, such as Åbo Akademi University [30,31], Aston University [32,33], and National Renewable Energy Laboratory [34]. ZSM-5 plays an essential role in each case, and is almost omnivorous for different feedstocks.

Unlike the catalytic pyrolysis of biomass and its derivatives, relatively few studies investigate the catalytic pyrolysis of furfural, especially in a fast pyrolysis environment. The Dao group [35,36] studied glucose-related compounds, including furfural, over ZSM-5-based catalysts. They achieved poor yields of hydrocarbon products (less than 10%), with mostly furan and CO derived from furfural decarbonylation. Grandmaison et al. [37] employed ZSM-5 in both furfural and furan conversion, proving that the latter was more stable than the former. Nevertheless, converting furanic

* Corresponding author. Tel.: +886 3 463 8800x3554; fax: +886 3 455 9373.
E-mail address: yclin@saturn.yzu.edu.tw (Y.-C. Lin).

0926-860X/$ – see front matter © 2012 Elsevier B.V. All rights reserved.
doi:10.1016/j.apcata.2012.01.017

compounds resulted in low hydrocarbon yields with long contact times (more than 1000 s). The Huber group lately performed furan and furfural conversion in both batch and continuous systems with short contact times [38–40], and achieved more than a 30% yield of aromatics. They also demonstrated that the product distribution can be manipulated using the appropriate operating conditions.

This study investigates the catalytic pyrolysis of furfural in producing gasoline-range fuels. The effects of reactant contact time, pyrolysis temperature, and catalytic promoter were studied. ZSM-5-based catalysts, including H-ZSM-5 and Zn/H-ZSM-5, were employed in a fixed bed system. Zinc cations were introduced into H-ZSM-5 because of their capability in hydrogen atom transfer, which is a major factor in aromatization [41–44]. This study shows that it is possible to adjust the product distribution using catalyst design and reaction environments in a continuous catalytic pyrolysis system. This study also proposes a plausible mechanism of furfural pyrolysis.

2. Experimental

2.1. Material

Furfural (Sigma–Aldrich, ACS reagent, 99%) was used directly without purification. ZSM-5 (Zeolyst, CBV 8014) with a SiO_2/Al_2O_3 ratio of 80 was calcined in air at 600 °C overnight before treatment. H-ZSM-5 was synthesized using the ion-exchange method with a 1.0 M solution of NH_4NO_3 (Sigma–Aldrich, ACS reagent 99%) at 70 °C for 1 h. The residual was filtered, washed with deionized water, dried at 100 °C for 10 h, and calcined at 600 °C overnight. The resulting powder was labeled as H-ZSM-5. Zn/H-ZSM-5 was prepared using the incipient wetness impregnation with a 0.1 M $Zn(NO_3)_2$ solution. Approximately 0.5 and 1.5 wt% loadings of Zn were used. The remaining paste was dried in air at 100 °C for 10 h then calcined at 550 °C overnight.

2.2. Catalyst characterization

X-ray diffraction (XRD) patterns were recorded using a Shimadzu Labx XRD-6000 with Cu Kα radiation (0.15418 nm). Scans were taken at a 5–60° 2θ range with a scanning rate of 4°/min. The voltage and current used were 40 kV and 30 mA, respectively.

Ammonia pulse chemisorption and ammonia temperature-programmed desorption (NH_3-TPD) were performed in the same system [45]. The system consisted of a thermal conductive detector (TCD), a temperature-controlled furnace, and a U-shaped quartz cell. The pulse chemisorption of ammonia was carried out to estimate the number of acid sites on the catalysts. Each trial used approximately 30 mg of the sample. The sample was pretreated in a He stream at 120 °C for 30 min. Pulse chemisorption was executed by injecting 1% NH_3/He (10 mL) pulses through the catalyst bed at 130 °C until achieving breakthrough. NH_3-TPD was performed after NH_3 pulse chemisorption in a He stream from 130 to 650 °C with a 10 °C/min heating rate. Re-adsorption of NH_3 was evaluated by varying the contact time of the carrier gas as Fig. S1 shows (see supplementary data). The re-adsorption effect can be ignored at a carrier gas contact times of less than 5×10^{-4} g/min/mL in this case, the first and second desorption temperatures were nearly identical with decreasing contact times. Therefore, a contact time of 5×10^{-4} g/min/mL was selected for all NH_3-TPD experiments. The baseline drift of pulse chemisorption and NH_3-TPD was evaluated by blank runs.

Temperature-programmed oxidation (TPO) was conducted using a thermogravimetric analyzer (TGA, TA Instruments Q50). Approximately 6 mg of post-reaction catalyst was placed in a platinum pan for each trial. The sample was dehydrated at 120 °C for an hour prior to the test. The pre-treated sample was subjected to a thermal program with a 5 °C/min heating rate in air (60 mL/min).

2.3. Activity evaluation

Catalytic performance was conducted using a continuous fixed bed design (Fig. 1). This system consisted of a quartz reactor (i.d. = 2 cm), a vapor saturator, a mass flow controller, and an ice bath cooling trap. The saturator was kept at 40 °C (furfural vapor pressure, ~743 Pa) using a water bath. The reaction temperature was controlled by a PID controller with a K-type thermal couple as the sensor and heavy duty heating tape (Omega) as the heat source. Prior to each test, blank runs were performed to evaluate the thermal cracking of furfural and to estimate the molar carbon input. Furfural decomposition was negligible (less than 5%) in the reaction environments. Three different temperatures (300, 400, and 500 °C) at gas hourly space velocity (GHSV) of 2412 h^{-1} and three different GHSVs (2412, 7200, and 36,000 h^{-1}) at 500 °C were applied to test all catalysts.

All catalysts were sieved to 40–80 mesh (0.42–0.18 mm) particle size. Each trial was carried out under atmospheric pressure with no pressure drop across the catalyst bed. About 0.2 g of catalyst was consumed per trial. All reactions reported were done with 13 min time on-stream. After reaction, stripping of catalyst was performed for 5 min using a N_2 stream of 25 mL/min. Gaseous products were collected in an air bag. Heavy products were trapped in the cooling trap. The condensed products were washed out with acetone before subsequent analysis. Qualitative and quantitative analyses of gas and liquid products were performed using a GC/MS (HP 5890 II GC with 5972 MSD, DB-5MS capillary column, 60 m × 0.25 mm) and a GC TCD/FID equipped with a methanizer (SRI 8610, molecular sieve 13X and silica gel columns). Standards such as benzene, toluene, phenol, furfural, *p*-xylene, benzofuran, naphthalene, and indene were injected into GC/MS; CH_4, CO, CO_2, ethylene, propylene, furan, benzene, toluene, and *p*-xylene were detected by GC TCD/FID. Because of a lack of standard reagents, the responses of methylnaphthalene and methylindene were set equal to naphthalene and indene; fluorene and anthracene, naphthalene. The resulting coke was analyzed by measuring the weight loss of spent catalyst using an elemental analyzer (EA, PerkinElmer series II 2400). The sample was treated in a 10% O_2/He stream at 150 °C for 30 min, followed by a 10 °C/min heating rate to 600 °C.

2.4. Soluble coke analysis

A leaching method developed by Guisnet and Magnoux [46] was conducted to identify the species preserved in the spent ZSM-5. Approximately 20 mg of used catalyst (H-ZSM-5 and 1.5% Zn/H-ZSM-5 in 500 °C, GHSV = 2412 h^{-1}) was soaked in 0.5 mL of 2% hydrofluoric acid at ambient temperature. After vigorous stirring for an hour, the sample was allowed to stand overnight. Soluble compounds were then extracted by adding 0.5 mL methylene chloride to the solution. The organic phase was then analyzed by GC/MS. Due to the lack of reference reagents, the GC/MS responses of extracted compounds (cyclohexene and 3,4-dimethylbenzaldehyde) were assumed to be the same as that of *p*-xylene.

3. Results and discussion

3.1. Physicochemical properties of catalysts

Fig. 2 depicts the XRD patterns of ZSM-5-based catalysts. Similar profiles were recorded for the investigated catalysts. This indicates that the crystalline structure of ZSM-5 remained intact after ion-exchange and Zn implementation. In addition, the characteristic

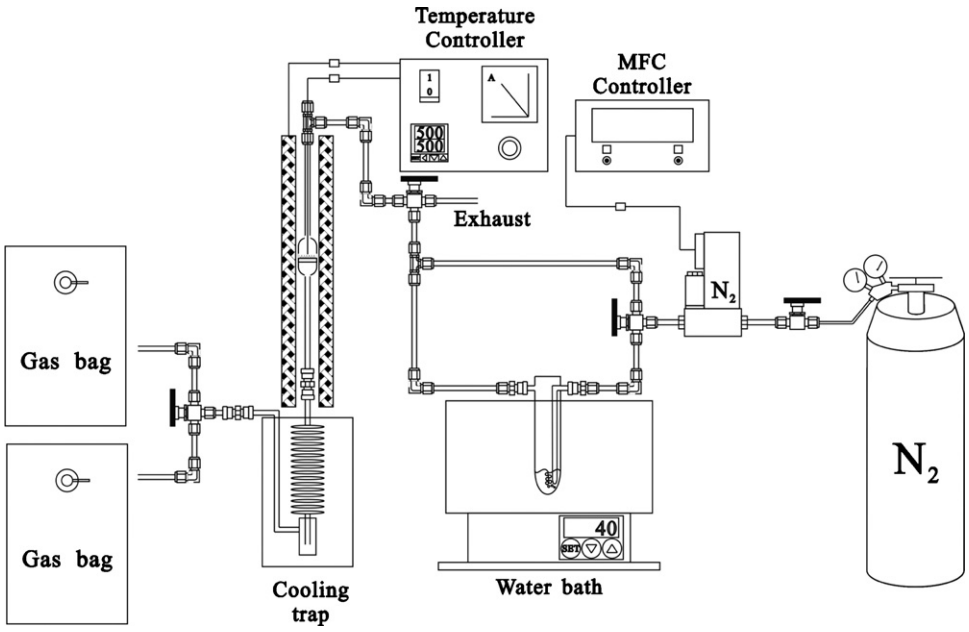

Fig. 1. Catalytic fast pyrolysis set-up.

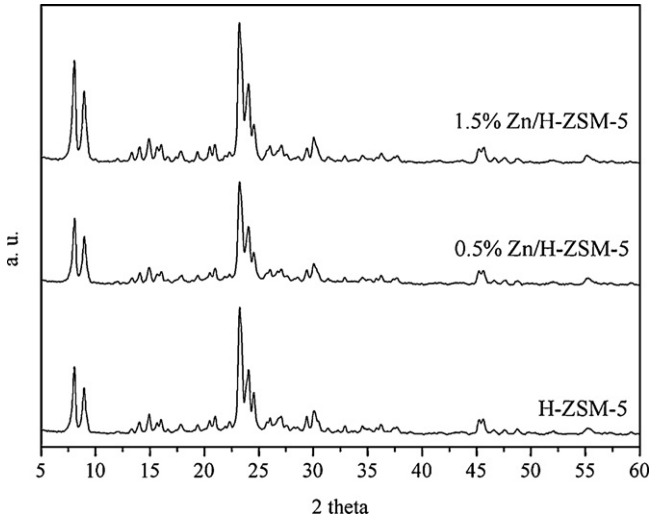

Fig. 2. XRD pattern of H-ZSM-5-based catalysts.

responses of ZnO were absent for 0.5 and 1.5% Zn/H-ZSM-5, suggesting that Zn ions were well dispersed. Various Zn species could coexist, such as Zn^{2+} replaces two protons with two aluminum sites (O^-—Zn—O^-) [41,47], zinc hydroxyl ($ZnOH^+$) [48], and finely dispersed ZnO [48].

Fig. 3 shows the NH_3-TPD profiles of freshly prepared catalysts. Table 1 summarizes the peak position, full width at half maximum (FWHM), acid site distribution, and the overall number of acid sites. Two desorption peaks are apparent. These peaks can be classified as weak and strong chemisorbed ammonia. The low desorption temperature (T_d) is associated with non-framework Lewis acid sites, whereas the high T_d is related to Brønsted acid sites on Si—O—Al groups [49].

Table 1
Characterization of acid sites of H-ZSM-5-based catalysts by NH_3-TPD.

Sample	Acid site type	Peak position (°C)	FWHM (°C)	Acid site content (%)	Total site (mmol/g)
H-ZSM-5	Lewis	177	47	16.2	0.36
	Brønsted	365	132	84.8	
0.5% Zn/H-ZSM-5	Lewis	198	88	29.4	0.37
	Brønsted	343	140	70.6	
1.5% Zn/H-ZSM-5	Lewis	216	98	47.2	0.39
	Brønsted	338	136	52.8	

As the Zn loading increased, the T_d of Lewis acid sites shifted from 177 to 216 °C. This suggests an increase in Lewis acidity. Moreover, increasing Zn content widened the FWHM of desorption response of Lewis sites, suggesting the presence of different Zn species [50]. In contrast, the T_d of Brønsted acid sites decreased from 365 to 338 °C with similar FWHMs. This implies that introduced Zn species suppressed the acidity of Brønsted acid sites. A possible explanation is that the introduction of Zn^{2+} exchanged the protons of Brønsted acid sites [41], leading to the decline of Brønsted acidity. The sum of Brønsted and Lewis acid sites increased following the trend of H-ZSM-5 ≤ 0.5% Zn/H-ZSM-5 ≤ 1.5% Zn/H-ZSM-5.

3.2. Reactivity of H-ZSM-5

Table 2 lists carbon yield and aromatic selectivity as functions of temperature for furfural pyrolysis over H-ZSM-5 at GHSV = 2412 h^{-1} (contact time = 1.5 s). Furfural was fully converted. As the temperature increased, aromatics increased from 0.1 to 15.7%; CO, 18.8 to 25.1%. Coke declined from 64.1 to 27.6%. The yield of furan initially increased from 16.5 to 30.6%, and then declined to 19.5%. Much greater amounts of ethylene, propylene, and CO_2 were detected at higher temperatures compared to low temperatures.

Based on their selectivity, aromatics can be categorized as mono-ring aromatics or polycyclic aromatic hydrocarbons (PAHs). Mono-ring products include benzene, toluene, phenol, and *p*-xylene, whereas PAHs include naphthalene, methylnaphthalene, indene, methylindene, benzofuran, fluorene, and anthracene. At low and moderate temperatures, the mono-ring species accounted for ~40%, and was mostly phenol and benzene. Naphthalene, methylnaphthalene, and benzofuran were the prominent products under the same environments. At the highest temperature, most aromatics are mono-ring species, and especially toluene. Heavy products such as fluorene and anthracene, which are

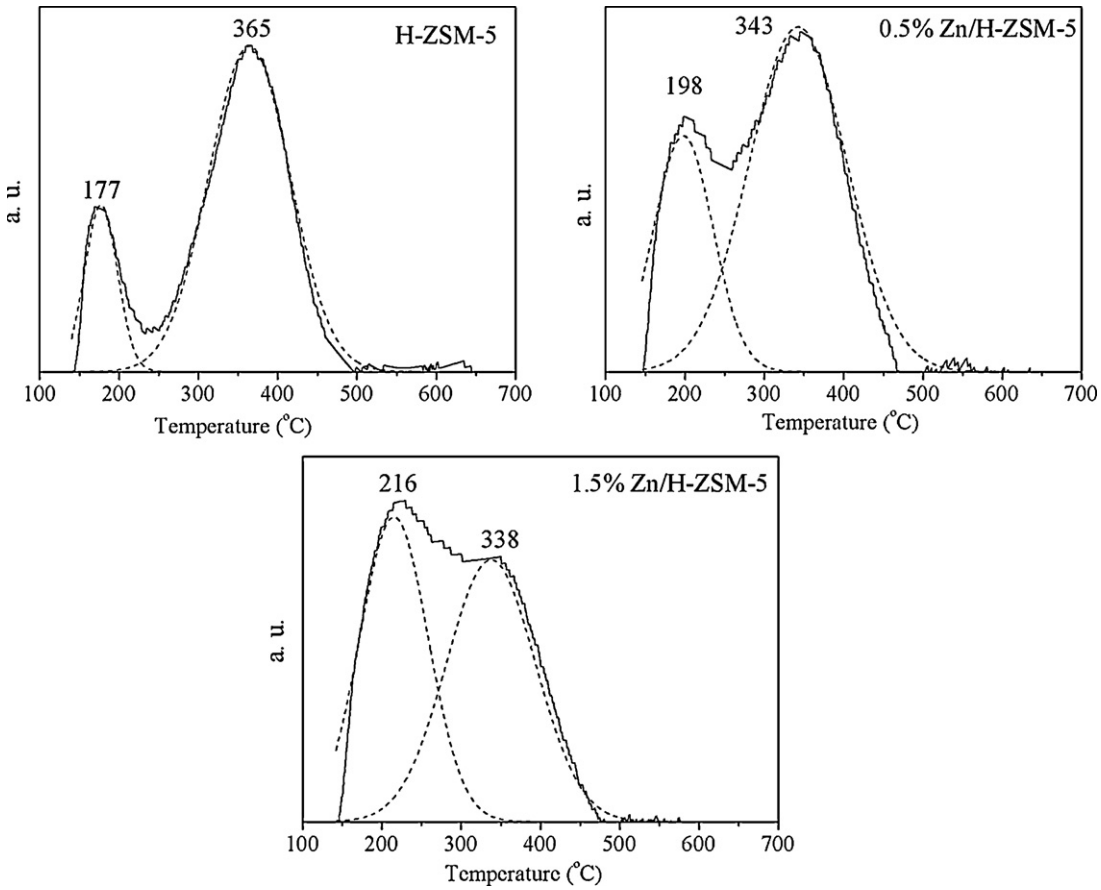

Fig. 3. NH_3-TPD of H-ZSM-5-based catalysts.

Table 2
Product carbon yield and aromatic selectivity as functions of temperature over H-ZSM-5.

	Temperature (°C)		
	300	400	500
Carbon yield (%)			
Aromatics	0.1	2.3	15.7
Coke	64.1	43.0	27.6
Furan	16.5	30.6	19.5
CO	18.8	20.8	25.1
CO_2	0.5	1.2	2.8
CH_4	0	0	0.1
C_2H_4	0	0.6	3.0
C_3H_6	0	0.3	3.1
Unidentified	0	1.2	3.1
Aromatic selectivity (%)			
Mono-rings			
Benzene	0	40.5	29.1
Toluene	0	0.1	62.2
p-Xylene	0	0	0
Phenol	44.2	3.7	0.2
PAHs			
Naphthalene	14.9	15.6	5.1
Methylnaphthalene	31.3	14.8	2.1
Indene	0.7	2.0	0.3
Methylindene	3.0	2.5	0.2
Benzofuran	3.6	19.4	0.2
Fluorene	1.2	0.5	0.2
Anthracene	1.1	0.9	0.4

Note that furfural was completely converted.

usually considered as coke precursors [40], decreased with increasing temperature. This agrees with the declining coke content.

Table 3 presents carbon yield and aromatic selectivity as functions of contact time over H-ZSM-5 at 500 °C. Furfural conversion was 100% for each trial. Excluding furan, all products showed a downward trend with decreasing contact time. This suggests that the outset of furfural conversion is the decarbonylation of furfural to furan and CO, followed by furan conversion to other products. With elevating contact times, the carbon yields of CO increased steadily from 20.4 to 25.1%. This indicates a subsequent route for furan decarbonylation to allene or methylacetylene [40].

Approximately 90% of mono-ring aromatics were generated at GHSVs of 2412–36,000 h^{-1} (contact time = 1.5–0.1 s). Benzene dominated at the shortest contact time. As the contact time increased, benzene decreased monotonically with increasing toluene. The same trend was observed for ethylene and propylene, indicating that benzene is the primary product of furan conversion. The formation of toluene and light olefins is highly correlated. The Diels–Alder cycloaddition of furan and light alkenes may be the source of PAHs [37]. However, this study provides no evidence supporting this hypothesis. This may be attributed to different pyrolysis environments: Kaliaguine and co-workers [37] employed a contact time thousands of orders of magnitude greater than in this study.

Fig. 4 shows the TPO signals of used H-ZSM-5 at 300, 400, and 500 °C. These profiles represent the combustion of deposited coke on the catalysts. According to Cheng and Huber [40], the TPO patterns represent the combustion of both oxygenated and graphite-like coke. Therefore, we deconvoluted the TPO pattern through Gaussian peak fitting using two or three peaks. The peak

Table 3
Product carbon yield and aromatic selectivity as functions of contact time over H-ZSM-5.

	GHSV (h^{-1})		
	2412	7200	36,000
Carbon yield (%)			
Aromatics	15.7	5.3	0.8
Coke	27.6	23.3	12.6
Furan	19.5	41.7	64.2
CO	25.1	23.4	20.4
CO_2	2.8	3.0	0.7
CH_4	0.1	0.1	0
C_2H_4	3.0	1.6	0.6
C_3H_6	3.1	1.6	0.6
Unidentified	3.1	0	0.1
Aromatic selectivity (%)			
Mono-rings			
Benzene	29.1	56.1	89.4
Toluene	62.2	42.1	0
p-Xylene	0	0	0
Phenol	0.2	0.2	0.4
PAHs			
Naphthalene	5.1	0.5	4.6
Methylnaphthalene	2.1	0.6	2.8
Indene	0.3	0.4	0.7
Methylindene	0.2	0.1	0.9
Benzofuran	0.2	0	0.3
Fluorene	0.2	0	0.4
Anthracene	0.4	0	0.5

Note that furfural was completely converted.

below 500 °C was regarded as oxygenated coke; beyond 500 °C, graphite-like coke. Table 4 summarizes the coke composition obtained by deconvoluting TPO. More and more graphite-like coke was formed as the reaction temperature increased. A visual observation (Fig. S2, supplementary data) further indicates that different types of coke were generated: after used at 300 °C, the surface was dark red. The surface then turned light gray after reaction at 500 °C. This agrees with earlier research [40], which shows the dark red color was the deposit of oligomerized furan, whereas the gray color is the graphite-like species.

Table 4
Deconvolution of TPO profiles of used H-ZSM-5 at different temperatures.

Reaction (°C)	Peak (°C)	Ratio	Coke type
300	334	0.09	Oxygenated coke
	435	0.36	Oxygenated coke
	518	0.55	Graphite-like coke
400	362	0.06	Oxygenated coke
	435	0.21	Oxygenated coke
	519	0.73	Graphite-like coke
500	–	0	–
	439	0.18	Oxygenated coke
	527	0.82	Graphite-like coke

3.3. Reactivity of Zn-promoted H-ZSM-5

Table 5 summarizes the product distributions of 0.5 and 1.5% Zn/H-ZSM-5 as functions of temperature. Furfural was completely converted. Like the trend observed for H-ZSM-5, aromatic yields were enhanced with increasing temperature at GHSV = 2412 h^{-1}. Furthermore, 1.5% Zn/H-ZSM-5 produced slightly higher aromatics (~5%) than 0.5% Zn/H-ZSM-5. Compared to untainted H-ZSM-5, Zn-doped H-ZSM-5 catalysts yielded greater aromatics and olefins with less furan and coke under the same reaction platforms. Furan was completely consumed for 1.5% Zn/H-ZSM-5 at 500 °C, GHSV = 2412 h^{-1}.

The selectivity of aromatics revealed different outcomes compared to pure H-ZSM-5. Although PAHs still dominated at the lowest temperature, benzene and toluene showed different trends

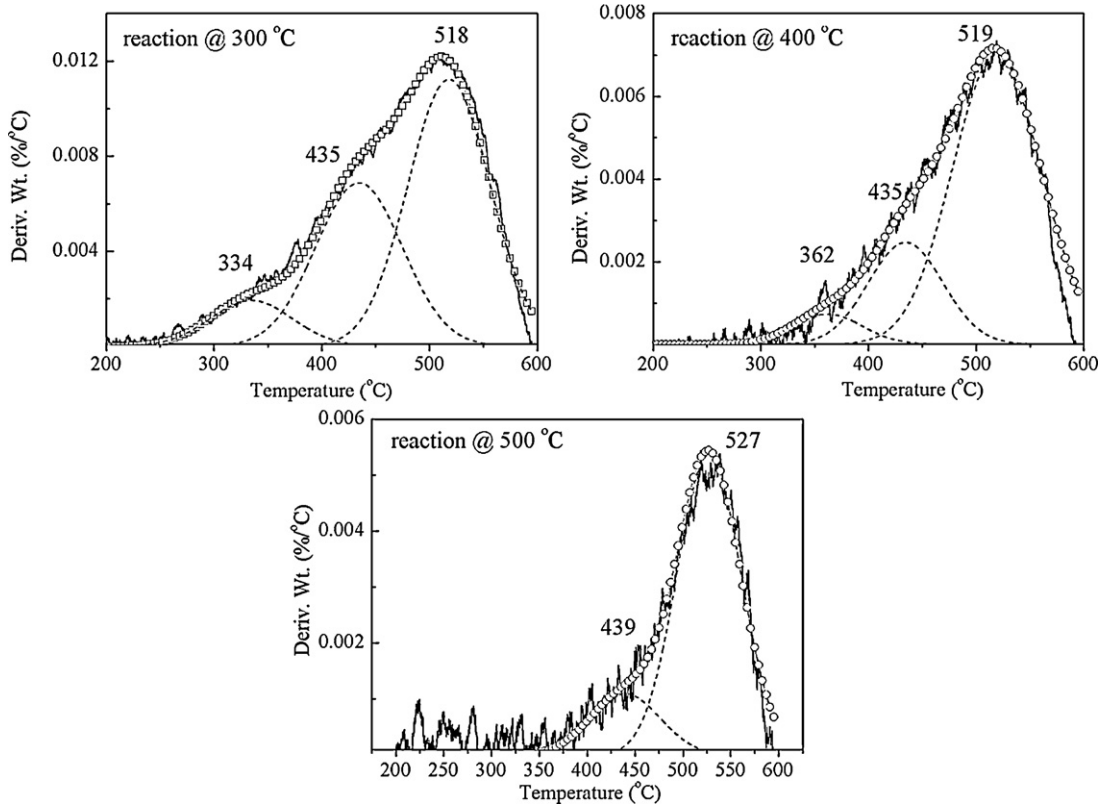

Fig. 4. TPO of post-reaction H-ZSM-5.

Table 5
Product carbon yield and aromatic selectivity as functions of temperature over 0.5% and 1.5% Zn/H-ZSM-5.

	Temperature (°C)					
	300		400		500	
	Zn (wt%)					
	0.5	1.5	0.5	1.5	0.5	1.5
Carbon yield (%)						
Aromatics	0.1	0	3.3	2.6	20.7	26.3
Coke	52.5	52.0	31.6	29.3	26.2	18.2
Furan	27.8	30.7	33.1	45.0	2.5	0
CO	18.5	16.2	18.5	19.2	28.2	28.8
CO_2	1.0	1.1	1.5	2.8	5.4	5.6
CH_4	0	0	0.1	0.2	2.9	3.3
C_2H_4	0	0	0.6	0.4	2.6	1.6
C_3H_6	0.1	0	0.5	0.5	1.5	1.2
Unidentified	0	0	10.8	0	10.0	15.0
Aromatic selectivity (%)						
Mono-rings						
Benzene	0	0	43.3	45.5	70.5	71.6
Toluene	0	0	45.7	35.5	26.5	25.0
p-Xylene	0	0	0	0	0	0
Phenol	6.5	10.4	0.6	0.5	0	0
PAHs						
Naphthalene	20.7	32.0	4.4	5.7	2.2	2.5
Methylnaphthalene	18.4	27.2	3.1	3.0	0.8	0.8
Indene	0.1	0	0	1.0	0	0.1
Methylindene	6.2	11.3	0.6	1.3	0	0
Benzofuran	46.6	19.1	1.7	6.1	0	0
Fluorene	0.8	0	0.3	0.7	0	0
Anthracene	0.7	0	0.3	0.7	0	0

Note that furfural was completely converted.

than H-ZSM-5: the former increased with elevating temperatures, whereas the latter decreased. This suggests that the alkylation of benzene and alkenes to toluene [40] was inhibited.

Table 6 lists the product distribution of 0.5 and 1.5% Zn/H-ZSM-5 at different contact times. No furfural was detected in the effluent.

Table 6
Product carbon yield and aromatic selectivity as functions of contact time over 0.5% and 1.5% Zn/H-ZSM-5.

	GHSV (h^{-1})					
	2412		7200		36,000	
	Zn (wt%)					
	0.5	1.5	0.5	1.5	0.5	1.5
Carbon yield (%)						
Aromatics	20.7	26.3	15.8	17.3	7.5	12.2
Coke	26.2	18.2	21.8	23.3	15.8	18.1
Furan	2.5	0	15.5	5.1	50.1	38.7
CO	28.2	28.8	24.3	24.8	22.5	24.2
CO_2	5.4	5.6	5.9	10.1	2.0	3.1
CH_4	2.9	3.3	2.0	3.7	0	0.9
C_2H_4	2.6	1.6	1.8	1.4	1.0	0.9
C_3H_6	1.5	1.2	2.0	1.8	1.1	1.2
Unidentified	10.0	15.0	10.9	12.5	0	0.7
Aromatic selectivity (%)						
Mono-rings						
Benzene	70.5	71.6	66.8	70.7	63.5	69.7
Toluene	26.5	25.0	31.4	27.4	34.9	28.9
p-Xylene	0	0	0	0	0	0
Phenol	0	0	0	0	0.1	0
PAHs						
Naphthalene	2.2	2.5	1.2	1.5	0.7	0.6
Methylnaphthalene	0.8	0.8	0.6	0.4	0.4	0.3
Indene	0	0.1	0	0	0.1	0.1
Methylindene	0	0	0	0	0.1	0.1
Benzofuran	0	0	0	0	0	0.1
Fluorene	0	0	0	0	0.1	0.1
Anthracene	0	0	0	0	0.1	0.1

Note that furfural was completely converted.

Table 7
Deconvolution of TPO profiles of used 0.5% Zn/H-ZSM-5 at different temperatures.

Reaction (°C)	Peak (°C)	Ratio	Coke type
300	335	0.08	Oxygenated coke
	418	0.40	Oxygenated coke
	505	0.52	Graphite-like coke
400	348	0.09	Oxygenated coke
	422	0.27	Oxygenated coke
	517	0.64	Graphite-like coke
500	–	0	–
	427	0.19	Oxygenated coke
	522	0.81	Graphite-like coke

As contact time decreased, the production of aromatics and coke declined, and furan became the prominent product. Unlike H-ZSM-5, ~10% aromatics were still generated by 1.5% Zn/H-ZSM-5 at the shortest contact time. Benzene and toluene, in approximately a 2:1 ratio, are two major species at 500 °C. 1.5% Zn/H-ZSM-5 produced slightly more benzene and less toluene than 0.5% Zn/H-ZSM-5. Again, increasing Zn content may retard the alkylation of benzene.

Figs. 5 and 6 display the TPO of post-reaction 0.5 and 1.5% Zn/H-ZSM-5. Tables 7 and 8 respectively show their peak position, coke composition, and coke type. The peak positions for different types of cokes were similar for all catalysts. However, as the Zn loading increased, less and less graphite-like coke was formed compared to those of H-ZSM-5. Moreover, the surface of 1.5% Zn/H-ZSM-5 turned light brown, instead of light gray, after used at 400 °C and above. For 1.5% Zn/H-ZSM-5, oxygenated coke became the prominent species on the catalyst surface. The TPO response of graphite-like coke cannot be specified in the post-reaction 500 °C sample.

Zinc-modified H-ZSM-5 has been extensively studied in aromatization of alkanes [41–44,48,50–52]. Aromatization is a sequence of hydride abstraction that generates carbenium ions as precursors of various products [43,51]. The Lewis acid sites newly-formed by zinc implementation stimulate H-atom migration (also called reverse spillover [43]) through C—H activation [42]. Activated hydrogen atoms are transferred to adsorbed carbenium by nearby Brønsted acid sites, which substantially enhance aromatics yields. The same could be stated in furfural conversion to aromatics: relatively high aromatics are produced by Zn-doped catalysts compared to parent H-ZSM-5. Moreover, the greater oxygenated coke by Zn/H-ZSM-5 implies a lower degree of dehydration (hydrogen loss) [40]. That is, more hydrogen atoms are available inside Zn-promoted zeolites for aromatization.

3.4. Soluble intermediates

Spent H-ZSM-5 and 1.5% Zn/H-ZSM-5 at 500 °C and 0.67 s^{-1} space time were subjected to leaching study as described in Section 2.4. Cyclohexene and 3,4-dimethylbenzaldehyde were identified as soluble intermediates. Nevertheless, these two contributed to less

Table 8
Deconvolution of TPO profiles of used 1.5% Zn/H-ZSM-5 at different temperatures.

Reaction (°C)	Peak (°C)	Ratio	Coke type
300	303	0.05	Oxygenated coke
	418	0.75	Oxygenated coke
	513	0.20	Graphite-like coke
400	299	0.04	Oxygenated coke
	425	0.82	Oxygenated coke
	530	0.14	Graphite-like coke
500	–	0	–
	480	1.0	Oxygenated coke
	–	0	–

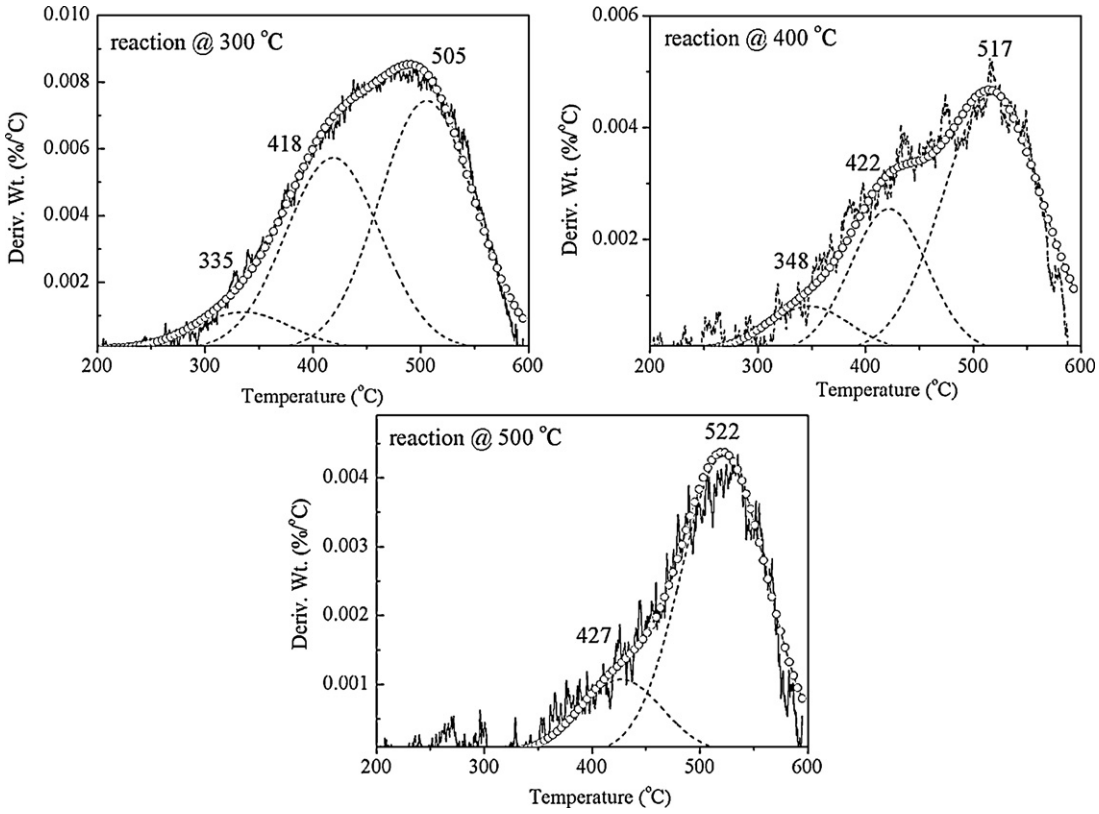

Fig. 5. TPO of post-reaction 0.5% Zn/H-ZSM-5.

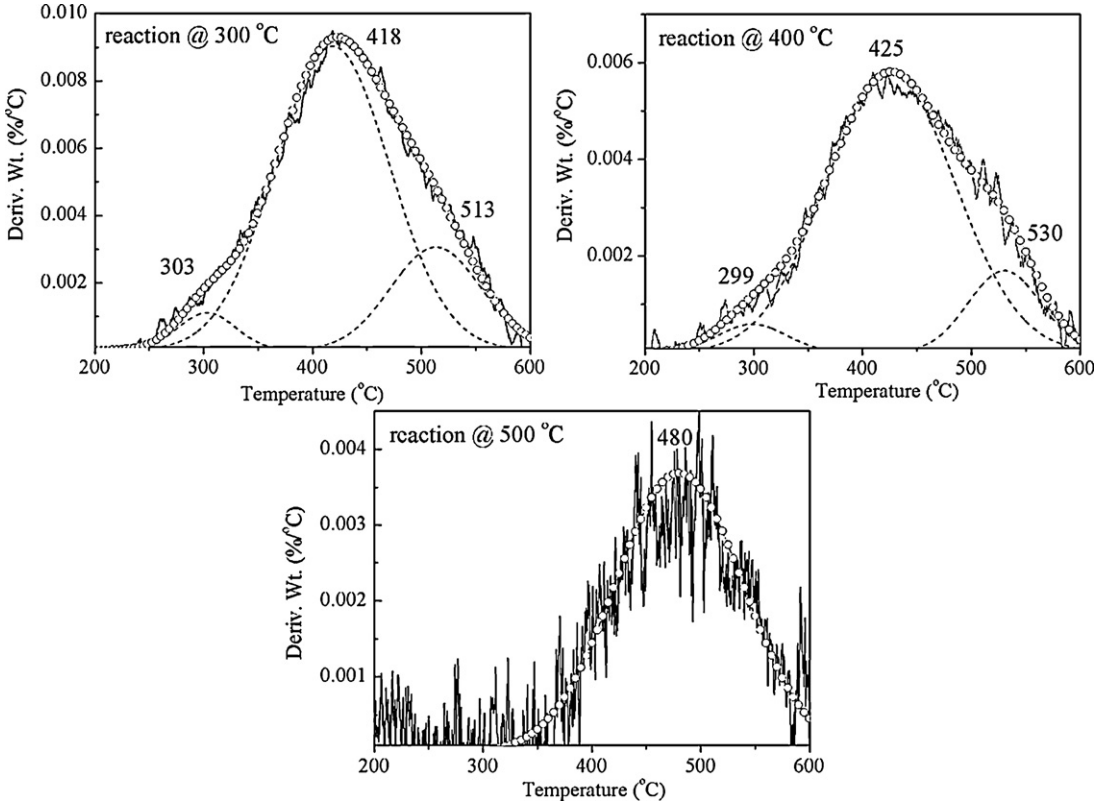

Fig. 6. TPO of post-reaction 1.5% Zn/H-ZSM-5.

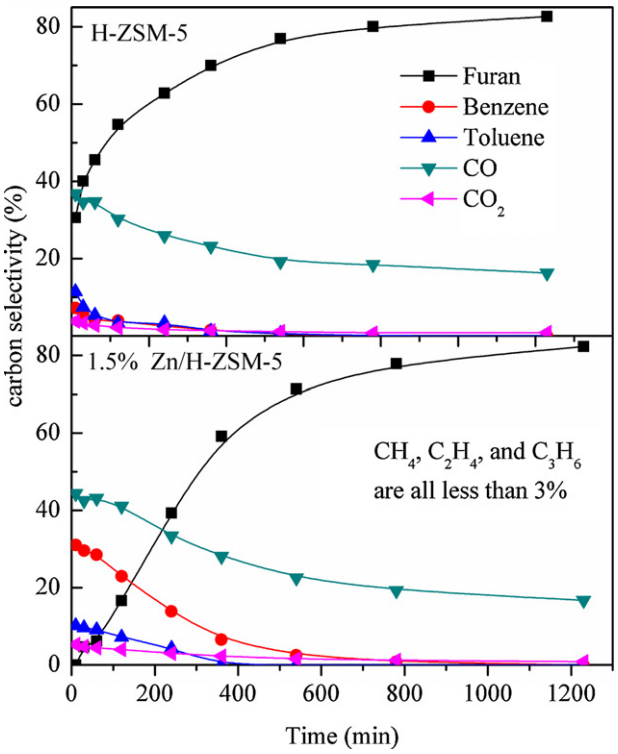

Fig. 7. Furfural conversion over H-ZSM-5 and 1.5% Zn/H-ZSM-5 as a function of time on-stream.

than 1% carbon yields of trapped species in both catalysts. Note that heavy compounds, which may have ~10^6 or higher molecular weights and cannot be detected by GC/MS, may be formed [40]. Advanced analysis using gel permeation chromatography (GPC) or ultraviolet-visible spectroscopy (UV–vis) should be able to provide more qualitative and quantitative information of retained species in ZSM-5.

3.5. Time on-stream testing

Fig. 7 displays the product distribution, except coke, as a function of time for H-ZSM-5 and 1.5% Zn/H-ZSM-5 at 500 °C and GHSV = 2412 h^{-1}. In both cases, furfural was fully converted in the testing period. Furan gradually increased with time on-stream, whereas CO, CO_2, benzene, and toluene decreased. At the outset, CO selectivity was similar for both catalysts; however, furan was completely converted on 1.5% Zn/H-ZSM-5, whereas approximately 30% furan was detected for H-ZSM-5. The former also displayed greater benzene selectivity (30%) than the latter (7%). Slightly higher toluene and CO_2 levels were also apparent on the Zn-doped H-ZSM-5. After 1000 min time on-stream, only furan and CO were identified at a 4:1 ratio. This indicates that furfural decarbonylation prevailed, and the active sites for aromatization were deactivated.

Fig. S3 (see supplementary data) shows the TPO patterns of spent H-ZSM-5 and 1.5% Zn/H-ZSM-5 at 500 °C, time on-stream studies. Again, graphite-like coke dominated on H-ZSM-5 whereas some oxygenated coke appeared on the 1.5% Zn/H-ZSM-5. Because furfural decarbonylation only occurred in the last stage, it is highly plausible that this reaction was catalyzed nonselectively. Different TPO profiles suggest diverse active phases produced by Zn substitution, promoting furan conversion to aromatics.

3.6. Reaction mechanism

According to the aforementioned outcomes, the mechanism of furfural catalytic fast pyrolysis can be proposed. The initiation of furfural conversion was decarbonylation, which liberates furan and CO as the products. This furan can then be transformed into intermediates inside the pores of ZSM-5-based catalysts. Leaching experiments indicate that parts of the intermediates are cyclohexene and 3,4-dimethylbenzaldehyde. Oxygenated coke can be formed concurrently from furfural or furan, particularly at low temperatures.

The intermediates in ZSM-5 cages can also be transformed into different products. At low temperatures, PAHs and oxygenated coke were the major products for all catalysts, with trace amounts of graphite-like coke. At high temperatures, H-ZSM-5 generated mono-ring aromatics, especially benzene, along with some light gases and graphite-like coke. The selectivities of toluene and light gases improved as the contact time increased. Therefore, the alkylation of benzene or other intermediates with alkenes may be a major pathway of toluene formation [39,40].

Incorporating zinc ions into H-ZSM-5 promoted the formation of benzene, light gases, and oxygenated coke at high temperatures. The yields of toluene and graphite-like coke declined as the zinc content increased, and graphite-like coke could not be detected at the highest amount of zinc loading. This indicates that zinc ions play a significant role in the aromatization of the intermediates within ZSM-5 pores; however, the activity of alkylation was suppressed. Different types of coke also suggest diverse pathways for untainted and promoted H-ZSM-5.

4. Conclusions

Furfural can be converted into aromatics by catalytic fast pyrolysis over ZSM-5-based catalysts. Reaction platforms and promoters are keys to manipulate the reaction pathway. Low temperatures favor the formation of PAHs and oxygenated coke, whereas high temperatures lead to mono-ring aromatics, light gases, and graphite-like coke. Zn-doped H-ZSM-5 can improve furan conversion, yielding more benzene, carbon oxides, and alkenes than untainted H-ZSM-5. H-atom transfer activity is the key for high aromatic yields. However, this inhibits the alkylation of benzene to toluene. This may be correlated to the Lewis acid sites newly synthesized by exchanged Zn cations. This study shows that furfural can be converted into valuable aromatics by continuous catalytic fast pyrolysis. The reaction temperature, reactant contact time, and catalytic promoter are critical factors in controlling the product distribution.

Acknowledgment

This work was sponsored by the National Science Council of Taiwan under grant #NSC 99-2221-E-155-075.

Appendix A. Supplementary data

Supplementary data associated with this article can be found, in the online version, at: doi:10.1016/j.apcata.2012.01.017.

References

[1] A.J. Ragauskas, C.K. Williams, B.H. Davison, G. Britovsek, J. Cairney, C.A. Eckert, W.J. Frederick Jr., J.P. Hallett, D.J. Leak, C.L. Liotta, J.R. Mielenz, R. Murphy, R. Templer, T. Tschaplinski, Science 311 (2006) 484–489.
[2] G.W. Huber, S. Iborra, A. Corma, Chem. Rev. 106 (2006) 4044–4098.
[3] Y.-C. Lin, G.W. Huber, Energy Environ. Sci. 2 (2009) 68–80.
[4] J.R. Salge, B.J. Dreyer, P.J. Dauenhauer, L.D. Schmidt, Science 314 (2006) 801–804.

[5] P.J. Dauenhauer, B.J. Dreyer, N.J. Degenstein, L.D. Schmidt, Angew. Chem. Int. Ed. 46 (2007) 5864–5867.
[6] T.R. Carlson, T.P. Vispute, G.W. Huber, ChemSusChem 1 (2008) 397–400.
[7] T.R. Carlson, G. Tompsett, W. Conner, G.W. Huber, Top. Catal. 52 (2009) 241–252.
[8] C. Branca, P. Giudicianni, C. Di Blasi, Ind. Eng. Chem. Res. 42 (2003) 3190–3202.
[9] D. Mohan, C.U. Pittman, P.H. Steele, Energy Fuels 20 (2006) 848–889.
[10] C. Di Blasi, C. Branca, A. Galgano, Ind. Eng. Chem. Res. 49 (2010) 2658–2671.
[11] B. Zhang, M. von Keitz, K. Valentas, Biotechnol. Bioeng. 101 (2008) 903–912.
[12] D.C. Elliott, T.R. Hart, Energy Fuels 23 (2009) 631–637.
[13] M. Joyce, US DOE, Development in U.S. Alternative Fuel Market, http://www.eia.doe.gov/cneaf/alternate/issues_trends/altfuelmarkets.html#pseries (accessed 14.11.2011).
[14] G.W. Huber, J.N. Chheda, C.J. Barrett, J.A. Dumesic, Science 308 (2005) 1446–1450.
[15] G.W. Huber, J.A. Dumesic, Catal. Today 111 (2006) 119–132.
[16] R. Xing, A.V. Subrahmanyam, H. Olcay, W. Qi, G.P. van Walsum, H. Pendse, G.W. Huber, Green Chem. 12 (2010) 1933–1946.
[17] C.D. Chang, A.J., Silvestri, R.L. Smith, Mobil Oil Corporation, U.S. patent 3 894 103, (1975).
[18] C.D. Chang, A.J. Silvestri, J. Catal. 47 (1977) 249–259.
[19] P.B. Weisz, W.O. Haag, P.G. Rodewald, Science 206 (1979) 57–58.
[20] N.Y. Chen, T.F. Degnan Jr., L.R. Koenig, Chemtech 16 (1986) 506–511.
[21] J.P. Diebold, H.L. Chum, R.J. Evans, T.A. Milne, T.B. Reed, J.W. Scahill, in: D.L. Klass (Ed.), Energy from Biomass and Wastes X, IGT Chicago and Elsevier Applied Sciences Publishers, London, 1987, p. 801.
[22] J.P. Diebold, J.W. Scahill, in: E.J. Soltes, T.A. Milne (Eds.), Pyrolysis Liquid from Biomass, ACS, Washington, DC, 1988, pp. 297–307.
[23] P.T. Williams, P.A. Horne, Biomass Bioenergy 7 (1994) 223–236.
[24] P.T. Williams, P.A. Horne, J. Anal. Appl. Pyrolysis 31 (1995) 15–37.
[25] P.A. Horne, P.T. Williams, J. Anal. Appl. Pyrolysis 34 (1995) 65–85.
[26] P.A. Horne, P.T. Williams, Fuel 75 (1996) 1051–1059.
[27] S.P.R. Katikaneni, J.D. Adjaye, N.N. Bakhshi, Energy Fuels 9 (1995) 1065–1078.
[28] J.D. Adjaye, N.N. Bakhshi, Fuel Process. Technol. 45 (1995) 161–183.
[29] J.D. Adjaye, N.N. Bakhshi, Fuel Process. Technol. 45 (1995) 185–202.
[30] A. Aho, N. Kumar, K. Eränen, T. Salmi, M. Hupa, D.Y. Murzin, Fuel 87 (2008) 2493–2501.
[31] A. Aho, N. Kumar, A.V. Lashkul, K. Eränen, M. Ziolek, P. Decyk, T. Salmi, B. Holmbom, M. Hupa, D.Y. Murzin, Fuel 89 (2010) 1992–2000.
[32] A. Pattiya, J.O. Titiloye, A.V. Bridgwater, J. Anal. Appl. Pyrolysis 81 (2008) 72–79.
[33] A. Pattiya, J.O. Titiloye, A.V. Bridgwater, Fuel 89 (2010) 244–253.
[34] R. French, S. Czernik, Fuel Process. Technol. 91 (2010) 25–32.
[35] L. Dao, M.I. Haniff, A. Houle, D. Lamothe, Am. Chem. Soc., Div. Fuel Chem. Prepr. 32 (1987) 308.
[36] M.I. Haniff, L.H. Dao, Appl. Catal. 39 (1988) 33–47.
[37] J.-L. Grandmaison, P.D. Chantal, S.C. Kaliaguine, Fuel 69 (1990) 1058–1061.
[38] T.R. Carlson, J. Jae, Y.-C. Lin, G.A. Tompsett, G.W. Huber, J. Catal. 270 (2010) 110–124.
[39] T.R. Carlson, Y.-T. Cheng, J. Jae, G.W. Huber, Energy Environ. Sci. 4 (2011) 145–161.
[40] Y.-T. Cheng, G.W. Huber, ACS Catal. 1 (2011) 611–628.
[41] J.A. Biscardi, G.D. Meitzner, E. Iglesia, J. Catal. 179 (1998) 192–202.
[42] J.A. Biscardi, E. Iglesia, J. Catal. 182 (1999) 117–128.
[43] C.P. Nicolaides, N.P. Sincadu, M.S. Scurrell, Catal. Today 71 (2002) 429–435.
[44] L.M. Lubango, M.S. Scurrell, Appl. Catal., A 235 (2002) 265–272.
[45] C.-L. Li, Y.-C. Lin, Catal. Lett. 140 (2010) 69–76.
[46] M. Guisnet, P. Magnoux, Appl. Catal. 54 (1989) 1–27.
[47] V.I. Yakerson, T.V. Vasina, L.I. Lafer, V.P. Sytnyk, G.L. Dykh, A.V. Mokhov, O.V. Bragin, K.M. Minachev, Catal. Lett. (1989) 339–345.
[48] H. Berndt, G. Lietz, J. Völter, Appl. Catal., A 146 (1996) 365–379.
[49] G.L. Woolery, G.H. Kuehl, H.C. Timken, A.W. Chester, J.C. Vartuli, Zeolites 19 (1997) 288–296.
[50] H. Berndt, G. Lietz, B. Lücke, J. Völter, Appl. Catal., A 146 (1996) 351–363.
[51] M.S. Scurrell, Appl. Catal. 41 (1988) 89–98.
[52] T. Mole, J.R. Anderson, G. Creer, Appl. Catal. 17 (1985) 141–154.